1-12-2017

Omecamtiv Mecarbil Enhances the Duty Ratio of Human β-Cardiac Myosin Resulting in Increased Calcium Sensitivity and Slowed Force Development in Cardiac Muscle

Anja M. Swenson
Pennsylvania State University

Wanjian Tang
Pennsylvania State University

Cheavar A. Blair
University of Kentucky, cheavar41@uky.edu

Christopher M. Fetrow
Pennsylvania State University

William C. Unrath
Pennsylvania State University

See last page for additional authors

Authors
Anja M. Swenson, Wanjian Tang, Cheavar A. Blair, Christopher M. Fetrow, William C. Unrath, Michael J. Previs, Kenneth S. Campbell, and Christopher M. Yengo

Omecamtiv Mecarbil Enhances the Duty Ratio of Human β-Cardiac Myosin Resulting in Increased Calcium Sensitivity and Slowed Force Development in Cardiac Muscle

Notes/Citation Information
Published in *The Journal of Biological Chemistry*, v. 292, no. 9, p. 3768-3778.

Digital Object Identifier (DOI)
https://doi.org/10.1074/jbc.M116.748780

THE JOURNAL OF BIOLOGICAL CHEMISTRY VOL. 292, NO. 9, pp. 3768–3778, March 3, 2017

Omecamtiv Mecarbil Enhances the Duty Ratio of Human β-Cardiac Myosin Resulting in Increased Calcium Sensitivity and Slowed Force Development in Cardiac Muscle*[S]

Received for publication, July 16, 2016, and in revised form, January 5, 2017 Published, JBC Papers in Press, January 12, 2017, DOI 10.1074/jbc.M116.748780

Anja M. Swenson[‡], Wanjian Tang[‡], Cheavar A. Blair[§], Christopher M. Fetrow[‡], William C. Unrath[‡], Michael J. Previs[¶], Kenneth S. Campbell[§], and Christopher M. Yengo[‡1]

From the [‡]Department of Cellular and Molecular Physiology, Pennsylvania State University College of Medicine, Hershey, Pennsylvania 17033, the [§]Department of Physiology and Division of Cardiovascular Medicine, University of Kentucky, Lexington, Kentucky 40536-0298, and the [¶]Department of Molecular Physiology and Biophysics, Cardiovascular Research Institute, University of Vermont, Burlington, Vermont 05405

Edited by Velia M. Fowler

The small molecule drug omecamtiv mecarbil (OM) specifically targets cardiac muscle myosin and is known to enhance cardiac muscle performance, yet its impact on human cardiac myosin motor function is unclear. We expressed and purified human β-cardiac myosin subfragment 1 (M2β-S1) containing a C-terminal Avi tag. We demonstrate that the maximum actin-activated ATPase activity of M2β-S1 is slowed more than 4-fold in the presence of OM, whereas the actin concentration required for half-maximal ATPase was reduced dramatically (30-fold). We find OM does not change the overall actin affinity. Transient kinetic experiments suggest that there are two kinetic pathways in the presence of OM. The dominant pathway results in a slow transition between actomyosin·ADP states and increases the time myosin is strongly bound to actin. However, OM also traps a population of myosin heads in a weak actin affinity state with slow product release. We demonstrate that OM can reduce the actin sliding velocity more than 100-fold in the *in vitro* motility assay. The ionic strength dependence of *in vitro* motility suggests the inhibition may be at least partially due to drag forces from weakly attached myosin heads. OM causes an increase in duty ratio examined in the motility assay. Experiments with permeabilized human myocardium demonstrate that OM increases calcium sensitivity and slows force development (k_{tr}) in a concentration-dependent manner, whereas the maximally activated force is unchanged. We propose that OM increases the myosin duty ratio, which results in enhanced calcium sensitivity but slower force development in human myocardium.

Heart failure continues to be a major health problem worldwide, and despite current treatment options, the 5-year mortality rate remains relatively high (42%) (1, 2). In systolic heart failure, inotropic drugs, including β-agonists and phosphodiesterase inhibitors, are utilized to enhance cardiac muscle contractile force in individuals that are hypocontractile (3). However, prolonged use of these drugs is associated with increased myocardial oxygen demand, arrhythmias, and impaired calcium signaling (4, 5). Recently, drugs are being pursued that directly interact with cardiac myosin, the molecular motor that drives contraction in the heart, to enhance contractile force without altering intracellular calcium concentrations (6).

Muscle contraction is driven by an ATP-dependent cyclic interaction between the myosin thick filaments and actin thin filaments, with contraction and relaxation dependent on calcium-mediated changes in the thin filament regulatory proteins troponin/tropomyosin (7). Thick filament-associated proteins also play a role in regulating contraction (8, 9). A solid understanding of the conserved actomyosin ATPase pathway has emerged from decades of biochemical, biophysical, and structural studies (Scheme 1) (10, 11). ATP binding to actomyosin ($K'_1K'_2$) dramatically weakens the affinity of myosin for actin and rapidly dissociates the complex, which allows for ATP hydrolysis to occur in a detached state (K_3). Thus, the M·ATP and M·ADP·P_i states are referred to as weak actin binding states (boldface in Scheme 1), and the M·ADP and nucleotide-free states are referred to as strong actin binding states. The binding of M·ADP·P_i to actin triggers the myosin power stroke that is followed by an essentially irreversible phosphate release step (K'_4) (12, 13). A second power stroke is thought to occur after phosphate release but is controversial (before K'_{5A}) (12, 14). The release of ADP from the active site (K'_{5B}) is the step that limits detachment from actin and is thus thought to be the step that limits maximum shortening velocity in muscle (15). However, attachment-limited models have also been proposed that can explain maximum shortening velocity in the context of the myosin ATPase cycle (16, 17).

Omecamtiv mecarbil (OM)[2] is an allosteric modulator of human β-cardiac myosin that is currently in phase II clinical trials (18–20). OM was found to be specific for cardiac myosin

* This work was supported by American Heart Association Grant 14GRNT20380068 and National Institutes of Health Grant R01HL127699 (to C. M. Y.), American Heart Association Grant 15GRNT25460003 and National Institutes of Health Grant UL1TR000117 (to K. S. C.), and National Institutes of Health Grant R00HL124041 (to M. J. P.). The authors declare that they have no conflicts of interest with the contents of this article. The content is solely the responsibility of the authors and does not necessarily represent the official views of the National Institutes of Health.

[S] This article contains supplemental Fig. S1.

[1] To whom correspondence should be addressed: Dept. of Cellular and Molecular Physiology, Pennsylvania State College of Medicine, 500 University Dr., Hershey, PA 17033. Tel.: 717-531-8575; E-mail: cmy11@psu.edu.

[2] The abbreviations used are: OM, omecamtiv mecarbil; mant, *N*-methylanthraniloyl; ELC, essential light chain.

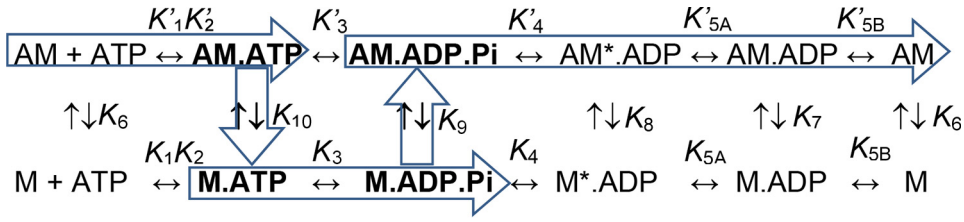

SCHEME 1

and does not alter skeletal or smooth muscle myosin (6). Muscle fiber studies that have examined the impact of OM are somewhat contradictory. A study that utilized rat cardiac muscle found enhanced contractility (fractional shortening) without changes in the calcium transient (6). Other studies have revealed an increase in calcium sensitivity as measured by the force-*p*Ca relationship in mouse and rat myocardium, but a slowing of force development and relaxation was also noted (21, 22). Only one study has examined human myocardium and found a slowing of cross-bridge kinetics and an increase in sensitivity to calcium (23).

To investigate how OM impacts cardiac myosin motor performance, studies have examined purified cardiac myosin using steady-state and transient kinetic analysis as well as *in vitro* motility assays (6, 24). A study on porcine cardiac myosin determined that OM alters the hydrolysis equilibrium constant to favor products and enhances the rate of actin-activated phosphate release, but it does not change the ADP release step (24). These factors were predicted to enhance the number of myosin cross-bridges in the strongly bound state, which would explain the increased force in muscle fiber studies. However, OM was found to decrease the maximum actin-activated ATPase rate (~2-fold) (24), but the step(s) in the ATPase cycle slowed by OM were not determined. Interestingly, it was found that OM dramatically reduces (10–20-fold) the sliding velocity in the *in vitro* motility assay (24–27). These results were puzzling because the study by Liu *et al.* (24) found no change in the ADP release rate constant, and this step correlates with sliding velocity in a detachment limited model of actomyosin motility. Thus, it has been proposed that the increase in the number of actin-bound cross-bridges enhances the load experienced by the force generating cross-bridges and slows the ADP release rate constant and hence sliding velocity (24). The ADP release step has indeed been demonstrated to be load-sensitive and responsible for the load-dependent changes in the ATPase rate in contracting muscle (28, 29). Therefore, further investigation of specific step(s) in the ATPase cycle that are slowed by OM is required to define the complete kinetic mechanism. In addition, it is important to directly measure the duty ratio, the fraction of the ATPase cycle myosin is bound to actin, in the *in vitro* motility assay to evaluate hypotheses about how OM dramatically slows sliding velocity. Finally, it is important to examine the impact of OM on human cardiac myosin as well as human cardiac muscle to allow direct correlations to clinical studies.

In this study, we investigated the mechanism of action of OM on recombinant human β-cardiac myosin using steady-state and transient kinetic measurements as well as *in vitro* motility assays. We also studied the impact of the drug on the muscle mechanics of human myocardium. We find that OM dramatically alters the myosin ATPase kinetics, which creates enhanced drag forces that contribute to the slowing of sliding velocity. Based on measurements with permeabilized human cardiac muscle, we find that OM increases calcium sensitivity and slows force generation, but it does not change steady-state force at saturating calcium concentrations.

Results

Purification of M2β-S1—We obtained ~0.75–1.0 mg of M2β-S1 per 30 plates of infected C_2C_{12} cells. The M2β-S1 was 95% pure based on Coomassie-stained SDS-polyacrylamide gels (Fig. 1). We assumed the two low molecular weight bands, which co-purified with the M2β-S1 heavy chain (99,021 kDa), corresponded to the myosin light chains. The low molecular weight bands were excised from the gel and digested into peptides using trypsin, and their sequences were determined using LC-MS/MS. The upper band generated unique peptides from two essential light chain isoforms as follows: nine peptides corresponding to 65% of the myosin light chain 1/3 (Myl1) sequence, skeletal muscle isoform (UniProt P05977), and 13 peptides corresponding to 55% of the myosin light chain 4 (Myl4) sequence, atrial/fetal isoform (UniProt P09541). The lower band generated 12 highly abundant unique peptides corresponding to 70% of the sequence of myosin regulatory light chain 2 (Mylpf), skeletal muscle isoform (UniProt P97457). The mouse essential light chains Myl1 and My14 were 75 and 79% identical and 83 and 91% similar, respectively, to the human cardiac muscle essential light chain (MYL3) (UniProt P08590). The mouse regulatory light chain contains 74% sequence identity and 87% sequence similarity with the human cardiac muscle regulatory light chain (MYL2) (UniProt P10916) (see supplemental Fig. S1 for alignments).

Actin-activated ATPase of M2β-S1—The maximum actin-activated ATPase rate and actin dependence of the ATPase rate of M2β-S1 were not significantly impacted by the presence of DMSO (0.1%) (Fig. 2*A* and Table 1). Biotinylation of the Avi tag of M2β-S1 also did not alter the ATPase activity. The presence of 10 μM OM reduced the maximal ATPase (k_{cat}) 4.5-fold and dramatically reduced the actin concentration at which ATPase is half-maximal (K_{ATPase}) 30-fold. The OM-induced inhibition of the actin-activated ATPase was evaluated in a concentration-dependent manner to determine the EC_{50} (0.52 ± 0.10 μM) (Fig. 2*B*).

Actin Co-sedimentation Assays with M2β-S1—We examined the steady-state actin affinity of M2β-S1 using actin co-sedimentation assays (Fig. 2*C*). The experiments were performed using conditions nearly identical to the ATPase assays with the exception that the co-sedimentation assay was performed over a longer time period (~10 min). The actin-affinity of M2β-S1 in

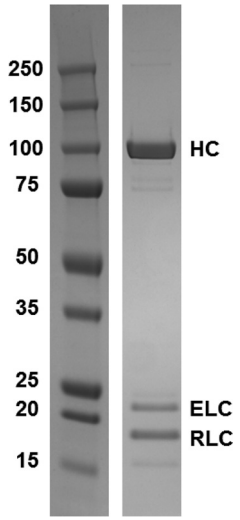

FIGURE 1. **Purified recombinant human M2β-S1.** Representative SDS-polyacrylamide gel of purified recombinant M2β-S1 compared with molecular weight standards as indicated. The myosin heavy chain (*HC*), regulatory (*RLC*), and essential light chains (*ELC*) are labeled.

the presence of ATP was similar in the presence and absence of OM (K_{actin} = 145 ± 18 and 155 ± 13 μM, respectively).

Transient Kinetic Analysis of Actin-activated Product Release—We examined the ADP release rate constant by mixing the actomyosin·mantADP complex (0.5 μM M2β-S1, 0.6 μM actin, 10 μM mantADP) with saturating ATP (1 mM), and we found that there was no difference in the presence and absence of OM (k_{obs} = 313 ± 6 and 306 ± 5 s^{-1}, respectively) (data not shown). We also performed single turnover sequential mix experiments in the stopped flow to monitor the actin-activated product release steps of M2β-S1 in the presence and absence of OM (Fig. 3). The experiment was performed by mixing M2β-S1 with substoichiometric mantATP, aging the reaction for 10 s to allow ATP binding and hydrolysis, and then mixing with varying concentrations of actin (0.25 μM M2β-S1, 0.23 μM mantATP, varying actin concentrations). We observed a two-exponential fluorescence transient at each actin concentration both in the presence and absence of OM (Fig. 3, *A–D*). The rate constant of the slow phase was independent of actin concentration and relatively similar in the presence and absence of OM (0.1–0.6 s^{-1}). The fast phase was hyperbolically dependent on actin concentration, and the maximum rate saturated at a much lower actin concentration in the presence of OM. In addition, the maximum rate constant of the fast phase was reduced in the presence of OM (4.3 ± 0.5 s^{-1}) compared with the absence (≥11.2 ± 0.1 s^{-1}). The relative amplitudes of the fast and slow phases were dependent on actin concentration with the fast phase more pronounced at a higher actin concentration (Fig. 3*C*). At high actin concentrations (40 μM), the relative amplitude of the slow phase was increased in the presence of OM (30%) compared with the absence (10%). Thus, the presence of OM slows actin-activated product release by reducing the rate constant of the fast pathway and increasing the flux through the slower product release pathway.

In Vitro Motility of M2β-S1—The sliding velocity produced by M2β-S1 in the *in vitro* motility assay was evaluated in the presence of DMSO and 10 μM OM by examining three separate protein preparations at a loading concentration of 0.48 μM (Fig. 4). There were slight differences in the average sliding velocity (50 filaments) determined in each preparation for the DMSO (1646 ± 30, 1837 ± 36, and 1469 ± 22 nm/s) and OM (7.87 ± 0.14, 6.50 ± 0.22, and 6.23 ± 0.19 nm/s) conditions. Control experiments performed in the absence of ATP demonstrated no movement during a 10-min acquisition (data not shown), which confirmed the sensitivity of the velocity measurements. Therefore, the data from all three preparations was pooled together (150 filaments) to determine the average sliding velocity in the presence of DMSO (1651 ± 24 nm/s) or OM (6.87 ± 0.12 nm/s). The average velocity of M2β-S1 was similar in the

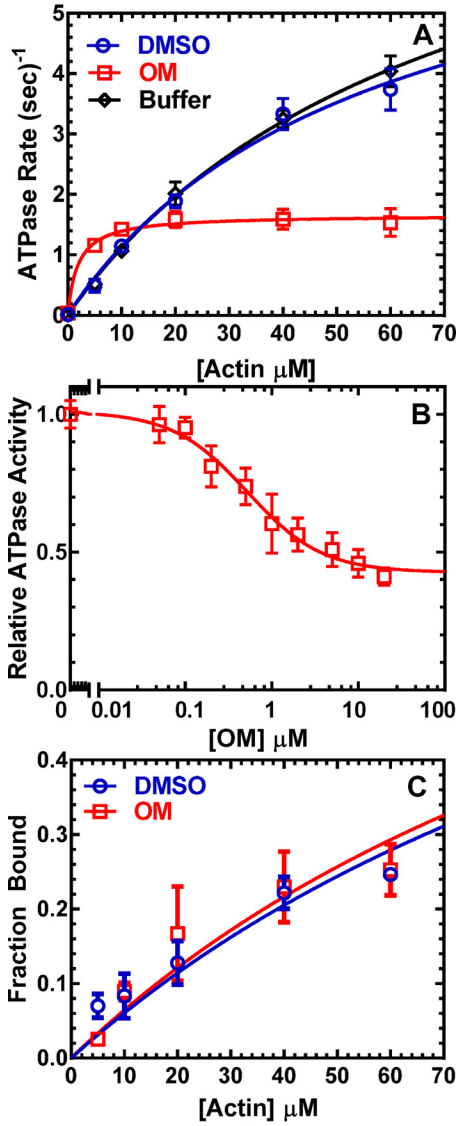

FIGURE 2. **Steady-state ATPase activity and actin affinity of M2β-S1 in the presence and absence of OM.** *A*, ATPase activity of M2β-S1 was examined as a function of F-actin concentration in MOPS20 buffer in the presence of 0.1% DMSO, 10 μM OM, or buffer only. The ATPase activity data were fit to a hyperbolic function to determine k_{cat} and K_{ATPase}. *B*, ATPase activity in the presence of 40 μM actin was examined in the presence of varying concentrations of OM. The data were fit to Equation 1 to determine the EC_{50}. *C*, steady-state actin affinity was measured in the presence and absence of OM using the actin co-sedimentation assay. The fraction of M2β-S1 bound to actin is plot as a function of actin concentration and fit to a hyperbolic equation to determine K_{actin}. *Errors bars* represent standard deviation of the mean from three protein preparations (some *error bars* are smaller than the symbol and therefore are not shown).

TABLE 1
Summary of actin-activated ATPase results with M2β-S1
ND means not determined.

Conditions	V_0	k_{cat}	K_{ATPase}
	s^{-1}	s^{-1}	μM
20 mM KCl[a]	0.02 ± 0.02	8.79 ± 0.56	69.88 ± 7.11
20 mM KCl (biotinylated)[b]	0.01 ± 0.01	7.36 ± 0.56	58.75 ± 5.59
20 mM KCl + DMSO[c]	0.02 ± 0.01	7.48 ± 1.07	56.53 ± 13.92
150 mM KCl + DMSO[d]	0.01 ± 0.01	ND	ND
20 mM KCl + OM[e]	0.04 ± 0.01	1.65 ± 0.05	1.91 ± 0.44
150 mM KCl + OM[f]	0.01 ± 0.01	1.46 ± 0.05	95.31 ± 63.0

[a] M2β-S1 is in MOPS 20 Buffer.
[b] Biotinylated M2β-S1 is in MOPS 20 Buffer.
[c] M2β-S1 in MOPS 20 Buffer is in the presence of 0.1% DMSO.
[d] M2β-S1 in MOPS (150 mM KCl) Buffer is in the presence of 0.1% DMSO.
[e] M2β-S1 in MOPS 20 Buffer is in the presence of 10 μM OM.
[f] M2β-S1 in MOPS (150 mM KCl) Buffer is in the presence of 10 μM OM.

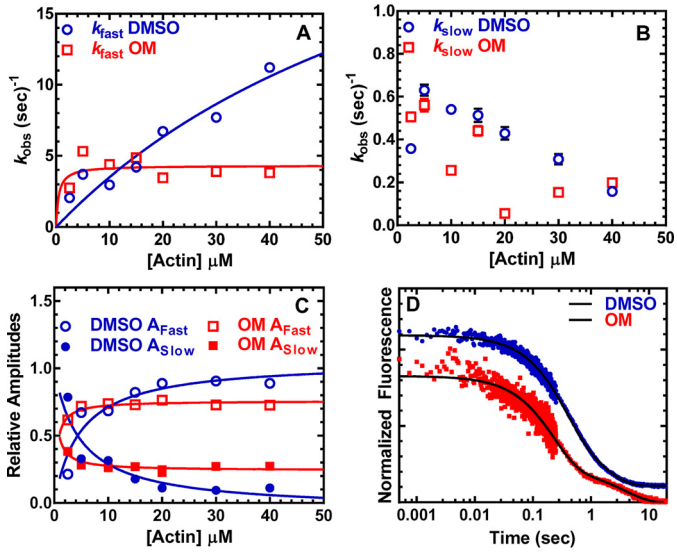

FIGURE 3. **Actin-activated product release of M2β-S1 in the presence and absence of OM.** A single turnover sequential mix stopped-flow experiment was performed by mixing M2β-S1 with substoichiometric mantATP, aged for 10 s, and then mixed with varying concentrations of actin. The fluorescence transients were best fit to a two-exponential function at all actin concentrations. *A,* fast phase of the fluorescence transients was plotted as a function of actin concentration and fit to a hyperbolic function. *B,* slow phase of the fluorescence transients ranged from 0.1 to 0.5 s^{-1}. *C,* relative amplitudes of the fast and slow components were plotted as a function of actin concentration and fit to a hyperbolic function. *D,* representative fluorescence transients obtained in the presence 10 μM actin and with (k_{obs} = 4.39 ± 0.10 and 0.26 ± 0.02 s^{-1}) or without (k_{obs} = 2.97 ± 0.01 and 0.63 ± 0.01 s^{-1}) OM. *Errors bars* represent standard error of the fits (some *error bars* are smaller than the symbol and therefore are not shown).

presence and absence (1712 ± 24 nm/s) of DMSO. The OM concentration-dependent inhibition of *in vitro* motility demonstrated that the EC_{50} was 5-fold lower (0.10 ± 0.01 μM) than that measured in the ATPase assay.

Ionic Strength Dependence of in Vitro Motility and ATPase Activity—The difference in the degree of OM-induced inhibition in ATPase and *in vitro* motility assays has also been demonstrated by two other groups and led them to propose that OM impacts strain-dependent ADP release in the motility assay (24–26). Based on our transient kinetic results, we reasoned that OM may promote a slow product release pathway that results in non-force generating heads, which create drag forces that contribute to the slowing of *in vitro* motility. We presumed that the slow pathway may stabilize the traditionally defined weak binding states (M·ATP or M·ADP·P_i). We tested this hypothesis by measuring the *in vitro* motility as a function of increasing ionic strength (20–150 mM KCl) in two protein preparations, because the weak binding states are known to be highly sensitive to ionic strength (Fig. 5 and Table 2) (30–32). We found that in the absence of OM, the increasing ionic strength results in little change in the velocity up to 100 mM KCl and a small reduction in velocity at 150 mM KCl (Fig. 5*A*). In the presence of OM, ionic strength increased the sliding velocity as indicated by more than a 2-fold increase demonstrated when comparing 20 and 150 mM KCl (Fig. 5*B*). We also found that the ATPase activity in the presence of 40 μM actin was more sensitive to ionic strength in the absence of OM, but in the presence of OM the ATPase was much less sensitive to the increase in ionic strength (Fig. 5*C*). In the presence of OM, we were able to determine the maximum ATPase activity at high ionic strength (150 mM KCl), although this was not feasible in the absence of OM (Table 1). Because the maximum ATPase rate was similar at high and low ionic strength, the enhanced sliding velocity observed at higher ionic strength is at least partially due to the attenuation of drag forces from weakly bound myosin heads.

Density Dependence of in Vitro Motility—We examined the density dependence of the sliding velocity by performing the *in vitro* motility assay as a function of M2β-S1 concentration loaded into the flow cell. At low ionic strength (MOPS20 buffer) in the absence of OM, we observed little change in the density dependence, but in the presence of OM, the velocity increased 2.5-fold as the loading concentration was decreased from 2.0 to 0.24 μM (Fig. 6, *A* and *B*). At higher ionic strength (100 mM KCl) in the absence of OM, the velocities gradually decreased as density was decreased, whereas in the presence of OM, the velocity increase at lower densities was attenuated compared with low ionic strength conditions.

Duty Ratio Measurements—To evaluate the hypothesis that OM increases the duty ratio, we attempted to directly examine the duty ratio in the *in vitro* motility assay (100 mM KCl) by examining the velocity as a function of available myosin heads on the surface (Fig. 7, *A* and *B*). We determined the number of heads on the motility surface using NH_4-ATPase assays (38 heads and 117 heads per μm of actin filament at 0.24 and 0.35 μM loading concentrations, respectively). We found it difficult to obtain sliding velocities at low motor density (≤10 available heads), and thus fitting the data to established equations (33, 34) was not robust. We did observe a trend in the data that demonstrated a relative increase in duty ratio in the presence of OM compared with DMSO. We also evaluated the duty ratio by plotting the velocity as a function of actin filament length at 0.24 μM loading concentration, and a similar trend was observed (Fig. 7*B*).

Muscle Mechanics of Human Myocardium—To evaluate the effects of OM on the contractile properties of human myocardium, we performed experiments using chemically permeabilized multicellular preparations. Maximum isometric force was not significantly altered by OM (Fig. 8*A*). In contrast, 1 and 10 μM OM significantly increased pCa_{50}, indicating that less free Ca^{2+} was required to produce half-maximal Ca^{2+} activation (Fig. 8*B*). These concentrations of OM also slowed k_{tr}, the rate of tension recovery following a rapid shortening/re-stretch perturbation (Fig. 8*C*). These data suggest that OM reduces the

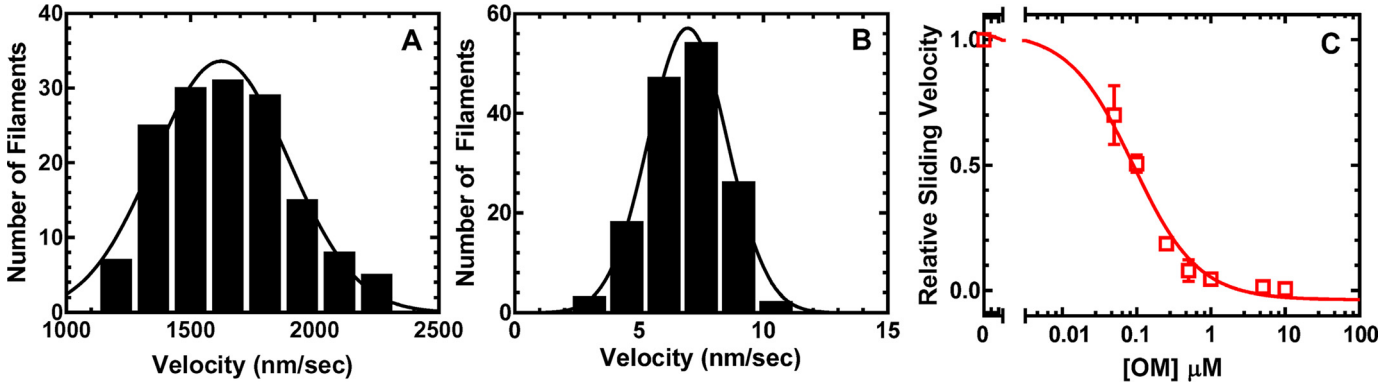

FIGURE 4. ***In vitro* motility of M2β-S1 in the presence and absence of OM.** The *in vitro* motility sliding velocity was determined for three different protein preparations in MOPS20 buffer in the presence of 0.1% DMSO (*A*) and 10 μM OM (*B*). The M2β-S1 loading density was 0.48 μM. The sliding velocities from all three preparations (150 filaments) were combined to determine the average velocity (nm/s) and standard error for the presence of DMSO (1651 $\pm$ 21) or OM (6.87 $\pm$ 0.12). *C*, sliding velocity was determined as a function of OM concentration and fit to Equation 1 to determine EC_{50}. *Errors bars* represent standard deviation of the mean from two protein preparations (some *error bars* are smaller than the symbol and therefore are not shown).

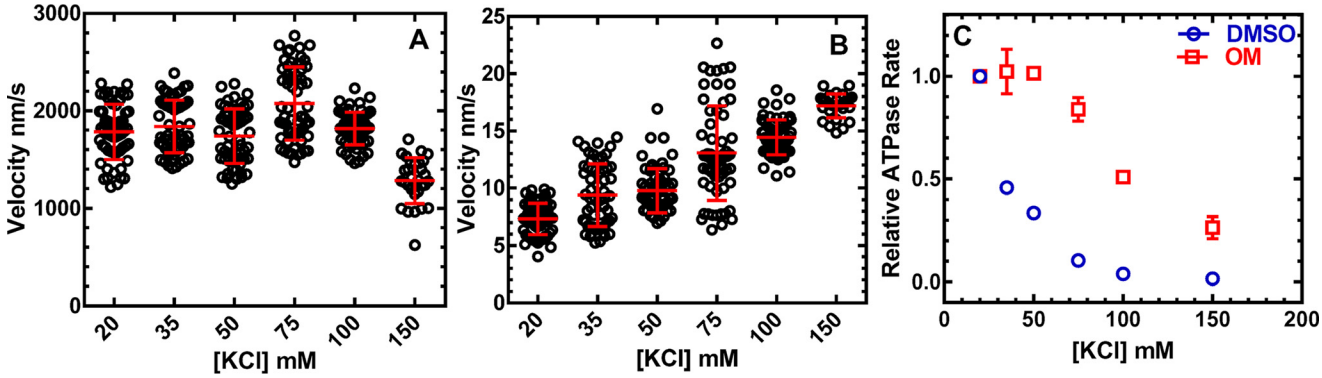

FIGURE 5. **Impact of ionic strength on the actin-activated ATPase and *in vitro* motility sliding velocity of M2β-S1.** The *in vitro* motility was measured as in Fig. 4 with the addition of the appropriate amount of KCl in the final activation buffer in the presence of 0.1% DMSO (*A*) or 10 μM OM (*B*). The M2β-S1 loading density was 0.48 μM, and an average velocity from 60 filaments analyzed is shown with a *red line*. *C*, ATPase activity was examined in the presence of 40 μM actin at different KCl concentrations with and without 10 μM OM. *Errors bars* represent standard deviation of the mean from two protein preparations (some *error bars* are smaller than the symbol and therefore are not shown).

TABLE 2

Summary of ionic strength dependence of *in vitro* motility assay results with M2β-S1

Conditions	Average sliding velocity	No. of filaments
	nm/s (±stderr)	
DMSO		
20 mM KCl	1783 ± 37	60
35 mM KCl	1839 ± 35	60
50 mM KCl	1739 ± 36	60
75 mM KCl	2074 ± 49	60
100 mM KCl	1817 ± 22	60
150 mM KCl	1284 ± 43	30
OM		
20 mM KCl	7.33 ± 0.18	60
35 mM KCl	9.39 ± 0.35	60
50 mM KCl	9.76 ± 0.25	60
75 mM KCl	13.07 ± 0.53	60
100 mM KCl	14.43 ± 0.20	60
150 mM KCl	17.17 ± 0.18	30

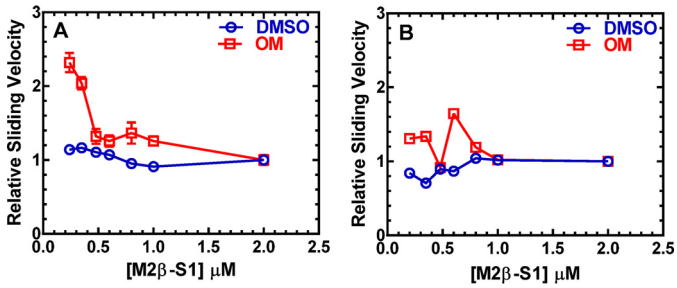

FIGURE 6. **Density dependence of *in vitro* motility of M2β-S1 in the presence and absence of OM.** We examined the sliding velocity as a function of M2β-S1 concentration loaded into the motility chamber (20 filaments/concentration). The average velocity (relative to the 2.0 μM loading concentration) at each loading concentration is plotted to demonstrate density dependence in low (20 mM KCl) ionic strength (*A*) and high (100 mM KCl) ionic strength (*B*). *Error bars* represent the standard error of the mean (some *error bars* are smaller than the symbol and therefore are not shown).

rate at which cross-bridges transition to force-dependent states in a dose-dependent manner.

Discussion

The discovery of drugs that directly interact with myosin to alter the force and velocity properties of cardiac muscle are promising, because they may be able to improve contractile performance without altering calcium homeostasis and myocardial oxygen demand. Our characterization of the motor properties of M2β-S1 suggests there are two kinetic pathways in the presence of OM. The drug can enhance the duty ratio of myosin heads that flux through the conserved ATPase pathway by increasing the period of time they are strongly bound to the actin filament during filament sliding. However, OM also traps some of the myosin heads in a weakly bound state with slow product release. We demonstrate that the main impact of OM

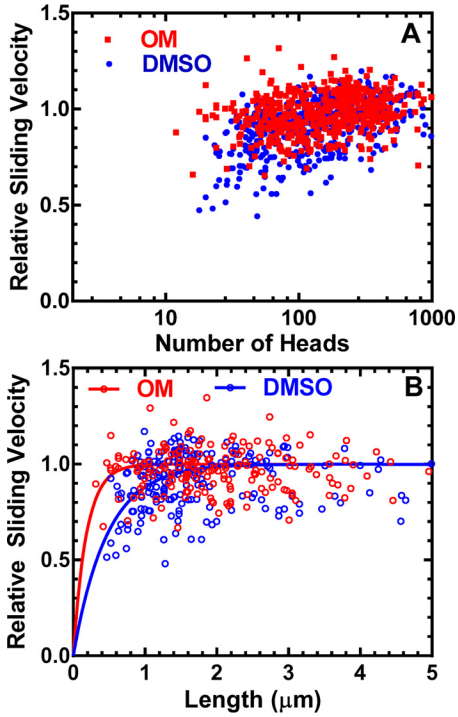

FIGURE 7. **Duty ratio of M2β-S1 in the presence and absence of OM.** *A*, we examined the duty ratio in the presence of DMSO and OM in high ionic strength buffer (100 mM KCl) by examining the sliding velocity as a function of available myosin heads (loading concentration was 0.24 or 0.35 μM). The number of available myosin heads was dependent on the density (determined with NH_4-ATPase assays) and the actin filament length. The trend in the data demonstrates a higher duty ratio in the presence of OM. *B*, velocity as a function of actin filament length (0.24 μM loading concentration) was also plotted, and the data are fit to a hyperbolic function to highlight the relative difference between the two conditions.

on human cardiac muscle mechanics is a shift in calcium sensitivity that is likely caused by the enhanced duty ratio that increases cooperative activation of the thin filament. In addition, OM slows down the kinetics of force development without changing steady-state force at maximum calcium concentrations.

Impact of OM on the Myosin ATPase Cycle in Solution—Our results add to the previous transient kinetic analysis of porcine cardiac heavy meromyosin and bovine cardiac myosin S1 in the presence of OM (6, 24). Similar to the previous findings, we found that when ADP release is measured by mixing a complex of actomyosin·ADP with excess ATP, the determined rate constant is nearly identical in the presence and absence of OM. This method likely monitors the final step of ADP release from actomyosin (K'_{5B}). We also examined actin-activated product release with sequential mix experiments and provide evidence for two product release pathways. The actin dependence of the rate constants of the fast phase from the sequential mix experiments (Fig. 3*A*, 70% of the amplitude at saturating actin) is very similar to the steady-state ATPase results (Fig. 2*A*). Thus, the fast phase likely represents the traditional pathway (Scheme 1, *blue arrows*) in which the M·ADP·P_i complex binds to actin and releases phosphate (K'_4) and then ADP (K'_{5A} and K'_{5B}). We propose that the presence of OM slows the flux through the traditional pathway by slowing the isomerization between actomyosin·ADP states (K'_{5A}). The actin dependence of the ATPase assay (K_{ATPase}) is thought to be mainly determined by the hydrolysis equilibrium constant as well as the rate constants for actin-activated phosphate release and ADP release (35). We find that the reduction in K_{ATPase} in the presence of OM is consistent with the previous transient kinetic studies (6, 24) and our current results that suggest K'_{5A} is reduced in the presence of the drug.

The slower pathway observed in our sequential mix experiments may be associated with slow ATP hydrolysis (K_3) or phosphate release (K_4). The slower pathway could be associated with the formation of strong or weak actin binding states, but because the actin co-sedimentation assay demonstrates that the steady-state actin affinity is unchanged by OM, we favor the latter. A previous transient kinetic study proposed a branched pathway associated with formation of a post-hydrolysis dead end intermediate with slow phosphate release (24). In this model, ATP hydrolysis occurs before formation of the pre-power stroke state, which leads to formation of myosin with hydrolyzed ATP in its active site but still in a post-power stroke state. We propose that OM increases the flux through this pathway and stabilizes the dead end intermediate that generates a pool of non-force generating heads. The proposed mechanism is consistent with the increased drag forces that are ionic strength-dependent in the motility assay. Our transient kinetic results are consistent with the 4–5-fold decrease in the maximum steady-state ATPase rate. Further transient kinetic analysis is necessary to directly examine the impact of OM on key steps in the ATPase pathway, including the affinity for actin in the weak binding states and the isomerization between actomyosin·ADP states (K'_{5A}).

Impact of OM on in Vitro Motility—We demonstrate that M2β-S1 in the absence of OM can generate sliding velocities that are 2-fold faster than the previous work with recombinant human β-cardiac myosin. Previous studies have found that the sliding velocity is between 800–1000 nm/s using a construct that contains only the essential light chain binding region and not the regulatory light chain (short S1) (26, 36, 37). The short S1 construct is attached to the surface with an antibody specific for a peptide added to the C terminus. Because this construct contains approximately one-half of the lever arm and the myosin lever arm length has been shown to correlate with step size and velocity (38–40), it is possible that the short lever arm reduces the sliding velocity. The Winkelmann laboratory (25) examined the sliding velocity of recombinant human cardiac motor domain with a GFP fusion in place of the lever arm that was attached to the surface with an anti-GFP antibody, and they found a sliding velocity of 800 nm/s. The same group also examined recombinant human cardiac heavy meromyosin directly attached to the surface and found the velocity was also 800 nm/s. The M2β-S1 used in this study was attached to the surface with an extremely high affinity interaction, streptavidin and biotinylated Avi tag, which may reduce nonspecific attachments of myosin with the motility surface. Previous studies have reported velocities from tissue-purified human cardiac myosin in the range of ~1500 nm/s (41), which is similar to our results. Our mass spectrometry revealed the presence of two ELC isoforms, which may also impact the sliding velocity. Indeed, a mouse model that induced overexpression of the atrial ELC isoform in the ventricle resulted in increased shortening velocity (1.78-fold) in isolated muscle and sliding velocity in

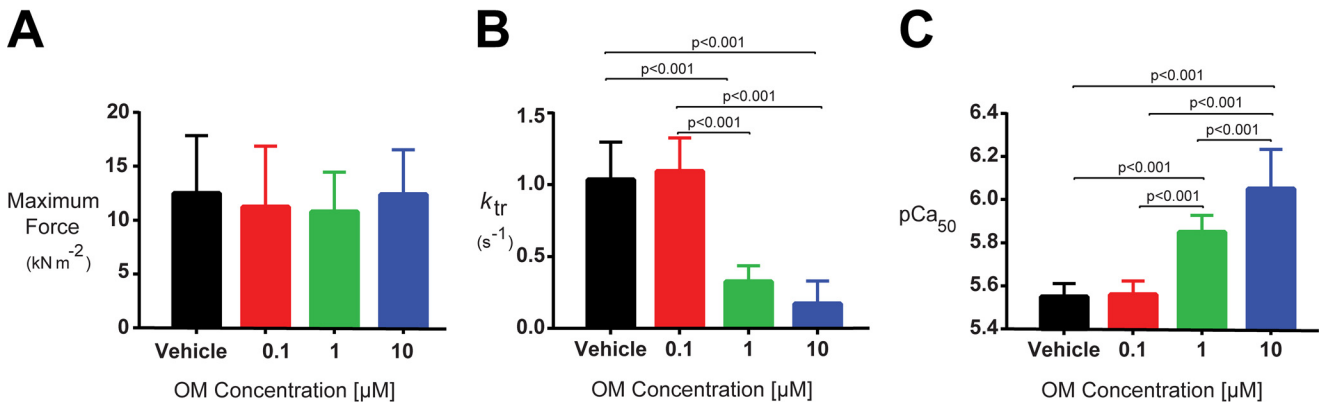

FIGURE 8. **Impact of OM on the contractile properties of human myocardium.** *A,* OM did not change the maximum force developed by human myocardium in solutions with a *p*Ca value of 4.5. *B,* OM decreased calcium sensitivity (pCa_{50}) in a dose-dependent manner. *C,* OM decreased the rate of force development (k_{tr}) in a dose-dependent manner.

the *in vitro* motility assays (1.17-fold) (42). Therefore, the differences in the velocities observed in this work compared with previous studies could be due to the methods of attaching the myosin to the surface, the length of the lever arm in the constructs examined, the light chain composition, and slight differences in the ionic strength and temperature utilized.

The large decrease in sliding velocity observed in the presence of OM in this study is more pronounced than the previous work with porcine and human cardiac myosin (15–20-fold) (24, 26, 27). One possible explanation for these differences is the higher velocities we observed in the absence of OM allowed for a larger OM-induced decrease to be observed as was found with α-cardiac myosin (26). However, the mechanism of how OM reduces the sliding velocity in the motility assay is still controversial. Our results suggest one major factor that could account for the large decrease in velocity in the presence of OM is the proposed reduction in the ADP isomerization step (K'_{5A}), which would increase the time myosin is attached to actin (t_{on}). If we assume a detachment limited model of sliding velocity ($V = d_{uni}/t_{on}$) (15) and no change in the unitary displacement (d_{uni}), then the velocity in the presence of OM is reduced proportionately to t_{on}. Therefore, it is important to examine d_{uni}, t_{on}, and the rate-limiting step in the M2β-S1 ATPase cycle to further evaluate this argument. Another possibility that has been proposed (24–26) is that OM increases the t_{on} of force generating cross-bridges by a strain-dependent ADP release mechanism. In this mechanism there is an internal load placed on the actin filament because of myosin heads that have completed their power stroke but are still attached to actin. The attached time of the force generating cross-bridges increases because they have to work against the internal load and adapt by slowing their ADP release rate constant. However, there is currently no direct evidence for changes in strain-dependent ADP release in the presence of OM.

We demonstrate the density dependence of *in vitro* motility is very unusual in the presence of OM, especially at low ionic strength. The trend of the increase in velocity at lower densities suggests that with fewer heads available there is a reduction in the drag forces that slow the velocity. These drag forces could come from post-power stroke strongly bound heads or weakly bound non-force generating heads. The weakly bound states are strongly affected by increases in ionic strength, which we demonstrate attenuates the OM-induced inhibition of actin sliding. Thus, our results suggest that the inhibition by OM can be attenuated by reducing the number of heads available to interact with the actin filament, which can be altered by changing the ionic strength or the motor density. Our results are consistent with a population of myosin heads trapped in a weak actin binding state that contributes to the drag forces that slow actin filament sliding. However, the sliding velocities observed at the highest ionic strength measured did not return the velocity to the values in the absence of OM. Thus, we propose that both the increase in t_{on} of force generating heads, by strain-dependent and/or non-strain-dependent mechanisms and drag forces from weakly bound non-force generating heads contribute to the reduced *in vitro* motility sliding velocity in the presence of OM.

Impact of OM on Cardiac Muscle Mechanics—Studies of the impact of OM on cardiac muscle mechanics are conflicting, but have some common findings. The initial studies fit well into a hypothesis that OM increases the rate of transition into the strong binding states and explains the enhanced force observed in the corresponding muscle fiber studies (6). Further studies on rat myocardium demonstrated an increase in calcium sensitivity with a slowed kinetics of force development and slowed relaxation (22). Recent studies have examined the impact of OM on human myocardium and found that OM increases isometric force at sub-maximal calcium concentrations and slows cross-bridge detachment and recruitment (23). Our study adds to these studies by further examining the impact of OM on human myocardium in a dose-dependent manner. We find an increase in calcium sensitivity with little change in steady-state force at maximum calcium concentrations. In addition, we observe a decrease in the rate of force development. We propose that the rate of force development could be altered by the weakly bound non-force generating cross-bridges or slow detachment of cross-bridges due to a slower ADP isomerization. The ionic strength of the muscle fiber experiments was slightly higher (180 mM) than the highest ionic strength in motility measurements where we still observed a large inhibition of the sliding velocity. Overall the muscle mechanic studies demonstrate that OM may help enhance force at lower calcium concentrations, whereas OM also has the potential to slow force development and reduce shortening velocity.

The results from clinical trials demonstrate that OM can improve systolic ejection time and stroke volume (18). However, end diastolic volume was reduced, which is in agreement with an impact on slowed relaxation kinetics. In addition, some patients experienced ischemia at higher doses. A larger phase II clinical trial found OM was well tolerated and confirmed previous reports of increases in systolic ejection time, although there was no improvement in the primary end point of dyspnea (20). Another study suggests OM causes an increase in oxygen consumption, which could impact bioenergetics in long term treatment regimens (43). Overall, it appears that dosing could be critical to receive the maximum benefits of the OM-induced increase in force at submaximal calcium without impacting the rate of force development and shortening velocity.

Summary—We have performed a thorough analysis of human M2β-S1 in the presence and absence of OM using both *in vitro* motility and solution ATPase studies. We complement this work with an investigation of the impact of OM on human cardiac muscle mechanics. Our results support a model that suggests OM slows ATPase cycle kinetics by slowing the transition between actomyosin·ADP states which results in an increase in duty ratio. OM also results in a population of cross-bridges trapped in a weak actin binding state with slow product release. The enhanced duty ratio increases the time period that myosin heads are attached to the thin filament in cardiac muscle which cooperatively activates the thin filament, enhances calcium sensitivity, and increases force at low calcium without changing steady-state force at maximum calcium. The negative impact of OM appears to be that it slows force development and could slow shortening velocity and may cause ischemia at high doses. Despite these potential drawbacks, an appropriate dose may provide a critical boost to contractile force in systolic heart failure patients. In addition, OM is an interesting proof of concept drug that may pave the way for future treatments that directly interact with contractile proteins to enhance the force and velocity properties of cardiac muscle.

Experimental Procedures

Reagents—ATP and ADP were prepared from powder (44). Omecamtiv mecarbil (CK-1827452) was purchased from Selleck Chemicals or AdooQ Bioscience. Omecamtiv mecarbil was dissolved in DMSO at a concentration of 10 mM. All solution experiments were performed in MOPS20 buffer (10 mM MOPS, pH 7.0, 20 mM KCl, 1 mM EGTA, 1 mM $MgCl_2$, 1 mM DTT) with the addition of appropriate KCl concentrations as indicated. 2′-Deoxy-ADP and 2′-deoxy-ATP labeled with *N*-methylanthraniloyl at the 3′-ribose position (mantADP and mantATP, respectively) were purchased from Jena Biosciences.

Construction of Expression Plasmids—The human cardiac myosin cDNA (AAA5187.1) was purchased from Thermo Fisher Scientific. PCR amplification was used to subclone the M2β-S1 construct (amino acids 1–843) into the pshuttle vector (a gift from Dr. Don Winkelmann). M2β-S1 was engineered to contain an N-terminal FLAG tag sequence and C-terminal Avi tag sequence.

Recombinant Adenovirus-based Expression and Purification of M2β-S1 in C_2C_{12} Cells—The production of high titer adenovirus was performed by a method developed in the Winkelmann laboratory (24, 45). Homologous recombination was used to produce pAdEasy recombinant adenovirus DNA (pAd.M2β-S1) by transforming the pshuttle.M2β-S1 into *Escherichia coli* BJ5183 cells. The pAd.M2β-S1 was transformed into XL-10 Gold cells for amplification, and the pAd.M2β-S1 DNA was digested with Pac1 and transfected into Ad293 cells to allow for virus packaging and amplification. The Ad293 cells were grown in DMEM supplemented with 10% fetal bovine serum. The large scale virus preparation was performed by infecting 60 plates (145 mm diameter). The virus was harvested with freeze-thaw cycles followed by CsCl density sedimentation. The final virus titers were typically 10^{10} to 10^{11} pfu/ml.

C_2C_{12} cells grown to 90% confluence in DMEM supplemented with 10% fetal bovine serum (typically 20–30 145-mm diameter plates) were differentiated by changing the media to DMEM supplemented with 10% horse serum and 1% fetal bovine serum. The C_2C_{12} cells were infected with recombinant adenovirus (5×10^8 pfu/ml) diluted into differentiation media. The media were changed after 2 days, and cells were harvested on day 7. The cells were lysed with a 50-ml Dounce in lysis buffer (50 mM Tris, pH 7.0, 200 mM KCl, 2 mM ATP, 1 mM ATP, 0.5% Tween 20, 0.01 mg/ml aprotinin, 0.01 mg/ml leupeptin, 1 mM PMSF) and spun two times for 15 min at 25,000 rpm in a Ti50 rotor at 4 °C. The supernatant was added to a 1-ml anti-FLAG M2 resin column, washed with wash buffer (10 mM Tris, pH 7.5, 200 mM KCl, 1 mM EGTA, 1 mM EDTA, 2 mM $MgCl_2$, 2 mM ATP, 1 mM DTT, 0.01 mg/ml aprotinin, 0.01 mg/ml leupeptin, 1 mM PMSF), and eluted with wash buffer containing FLAG peptide (0.167 mg/ml). The eluted M2β-S1 was subsequently precipitated with ammonium sulfate and dialyzed into MOPS20 buffer overnight at 4 °C. M2β-S1 was biotinylated for *in vitro* motility studies by incubating M2β-S1 with BirA (10 μg/ml) for 1 h at 25–30 °C, and subsequently precipitated with ammonium sulfate and dialyzed into MOPS20 buffer overnight at 4 °C (46).

M2β-S1 purity was assessed by Coomassie-stained SDS-polyacrylamide gels, and protein concentration was determined by Bradford assay using BSA as a standard. Similar results were obtained by measuring the absorbance and using the predicted extinction coefficient ($\epsilon_{280} = 1.38 \times 10^5\ M^{-1}{\cdot}cm^{-1}$). Actin was purified from rabbit skeletal muscle using an acetone powder method (47). The actin concentration was determined by absorbance at 290 nm ($\epsilon_{290} = 2.66 \times 10^4\ M^{-1}{\cdot}cm^{-1}$). A molar equivalent of phalloidin was added to stabilize F-actin.

Mass Spectrometry—Expression of M2β-S1 light chain isoforms was determined by liquid chromatography-tandem mass spectrometry (LC-MS/MS). The myosin light chains associated with the M2β-S1 were separated on SDS-polyacrylamide gels and stained by Coomassie. The two resultant low molecular mass bands (~22 and 19 kDa) were excised from the gel, destained with 50% acetonitrile, and digested with 1 μg of trypsin (Promega) in 50 mM ammonium bicarbonate as described (48). The resultant peptides were reconstituted in 0.05% heptafluorobutyric acid and separated on an Acquity UPLC HSS T3 column (100 Å, 1.8 μm, 1 × 150 mm) (Waters) attached to a Dionex UltiMate 3000 HPLC (Dionex). The HPLC effluent was directly injected into a Q Exactive Hybrid Quadrupole-Orbitrap mass spectrometer through an electrospray ionization source (Thermo Fisher Scientific). Data were collected in data-dependent MS/MS mode with the top five most abundant ions

being selected for fragmentation. Peptides were identified from the resultant MS/MS spectra by searching against a mouse database (downloaded from UniProt 2/15) using SEQUEST for running the Proteome Discoverer 2.1 software (Thermo Fisher Scientific). Peptide oxidation was accounted for by addition of 15.99 and 31.99 Da to each methionine residue. All MS/MS fragmentation spectra were manually confirmed. The area under each deisotoped LC peak was determined using Proteome Discoverer 2.1 (Thermo Fisher Scientific).

Steady-state ATPase Activity—Steady-state ATP hydrolysis by M2β-S1 (100 nM) in the absence and presence of actin (0–60 μM) was examined by using the NADH-linked assay (49–52) with a final MgATP concentration of 1 mM. The assay was performed in an Applied Photophysics stopped-flow apparatus (Surrey, UK) in which the NADH absorbance at 340 nm was monitored continuously for 200 s. The ATPase rate at each actin concentration was determined, and the Michaelis-Menten equation ($V_0 + (k_{cat}\,[actin])/(K_{ATPase} + [actin])$) was used to determine k_{cat} and K_{ATPase}, where V_0 is the ATPase rate in the absence of actin; k_{cat} is the maximal ATPase rate, and K_{ATPase} is the actin concentration at which the ATPase activity is half-maximal. The data at each actin concentration represents an average of 2–3 protein preparations.

Actin Co-sedimentation Assay—The steady-state actin affinity of M2β-S1 in the presence of ATP was measured using an actin co-sedimentation assay. M2β-S1 (0.2 μM) was equilibrated with various actin concentrations (0–60 μM) in MOPS20 buffer containing the ATP regeneration system (20 units·ml^{-1} pyruvate kinase and 2.5 mM phosphoenolpyruvate). We added 1 mM ATP and immediately centrifuged the samples for 8 min at 25 °C (TLA.120.1 rotor at 120,000 rpm). The supernatant and pellet were examined by SDS-PAGE followed by Western blotting, and the biotinylated M2β-S1 was detected using a streptavidin-alkaline phosphatase conjugate. The intensity of the M2β-S1 bands was examined using ImageJ, and the fraction bound was determined using the equation pellet/(supernatant + pellet). The plot of fraction bound as a function of actin concentration was fit to a hyperbolic function to determine the steady-state actin affinity (K_{actin}).

Transient Kinetic Studies—The stopped-flow apparatus equipped with an excitation monochrometer (2-nm band pass filter) and appropriate emission filters was used to examine key steps in the actomyosin ATPase cycle of M2β-S1. The mant-labeled nucleotides were excited at 290 nm, and the emission was measured with a 395-nm long pass filter. The fluorescence transients were fitted using custom software provided with the instrument or with GraphPad Prism, and errors are reported as standard errors of the fit. All concentrations listed are final unless otherwise noted.

In Vitro Motility Assay—The actin filament sliding assay was performed as described previously (53) except for the method of adhering the myosin to the surface. Microscope coverslips were coated with 1% nitrocellulose in amyl acetate (Ladd Research). The surface was coated with streptavidin (0.1 mg/ml) and blocked with BSA (1 mg/ml) before the addition of biotinylated M2β-S1 (loading concentration, amount added to the flow cell, was varied between 0.24 and 2.0 μM). Unlabeled actin (2 μM) followed by an ATP (2 mM) wash was used to prevent interactions with dead heads. Actin labeled with either rhodamine phalloidin (DS Red filter; excitation/emission: 545/620 nm) or Alexa (GFP filter; excitation/emission, 500/535 nm) was visualized by fluorescence microscopy. An activation buffer with an appropriate concentration of DMSO or OM was added to the flow cell to initiate motility. Activation buffer contained the following: MOPS20 buffer, 0.35% methylcellulose, 2.5 mM phosphoenolpyruvate, 20 units·ml^{-1} pyruvate kinase, 0.1 mg·ml^{-1} glucose oxidase, 5 mg·ml^{-1} glucose, 0.018 mg·ml^{-1} catalase, and 2 mM ATP. The slide was promptly viewed using a NIKON TE2000 microscope equipped with a ×60/1.4NA phase objective and a Perfect Focus System. Images were acquired every second for 3 min or every 15 s for 10 min in the absence and presence of OM, respectively, using a shutter-controlled Coolsnap HQ2-cooled CCD digital camera (Photometrics) binned 2 × 2. Temperature was maintained at 26 ± 1 °C and monitored using a thermocouple meter (Stable Systems International). Image stacks were transferred to ImageJ for analysis via MTrackJ (54) and corrected for drift using StackReg. The average velocity was determined by tracking actin filaments manually for each condition (*e.g.* the path of each filament was determined by tracking the filament on a frame-by-frame basis, which allowed determination of average velocity). The actin filament lengths were measured using the length tool in ImageJ.

The number of myosin heads on the motility surface was measured using an NH_4-ATPase assay (34, 55). We evaluated the number of moles of phosphate produced in a motility flow cell chamber and compared that with a standard curve of moles of phosphate produced per concentration of M2β-S1. To determine the number of heads available per μm of actin filaments, we assumed that M2β-S1 could interact with a 20-nm band of the actin filament (10 nm of either side of the filament). The plot of the relative velocity as a function of myosin heads available (33, 34) was utilized to demonstrate the relative difference in duty ratio in the presence of OM.

The plots of the relative ATPase and motility as a function of OM concentration were fit to Equation 1,

$$y = \text{Bottom} + (\text{Top-Bottom})/(1 + 10\hat{}(x - \log IC_{50})) \quad \text{(Eq. 1)}$$

where x = OM concentration, and y = relative ATPase activity or sliding velocity, and Bottom and Top are the associated plateaus.

Human Tissue—The cardiac samples used in this study were obtained from patients at the University of Kentucky who had end-stage heart failure using the procurement system described by Blair *et al.* (56). Briefly, through-wall sections of the distal anterior region of the left ventricle were obtained from hearts that had been explanted during a cardiac transplant. Samples weighing ~500 mg were dissected from these sections, placed in 2-ml cryogenic vials, and snap-frozen in liquid nitrogen. The vials were subsequently stored in the vapor phase of liquid nitrogen at −150 °C until use. The experiments described in this study used specimens isolated from the sub-endocardial region of eight patients. All procedures were approved by the

University of Kentucky Institutional Review Board, and the subjects gave informed consent.

Preparations and Experimental Setup—Multicellular preparations were obtained by mechanical disruption followed by chemical permeabilization using 1% v/v Triton X-100 detergent (57). Suitably sized preparations were attached between a force transducer (resonant frequency, 600 Hz; model 403, Aurora Scientific, Aurora, Ontario, Canada) and a motor (step time 0.6 ms; model 312B, Aurora Scientific) and stretched to a sarcomere length of 2.24 μm in a solution with a *p*Ca ($= -\log_{10}[Ca^{2+}]$) of 9.0. The mean length of the preparations was 1055 $\pm$ 229 μm. The cross-sectional area was $5.87 \pm 2.42 \times 10^{-8}$ m^2 (estimated assuming a circular profile). Experiments were conducted at 15 °C using SLControl software (58).

OM Preparation and Incubation of Samples—Solutions with *p*Ca values ranging from 9.0 to 4.5 and OM concentrations of 0.1, 1.0, or 10 μM were made by adding suitable amounts of OM dissolved in DMSO. The final percentage of DMSO in every experimental solution was 0.67%. Preparations were immersed in a *p*Ca 9.0 solution containing 0 (control), 0.1, 1.0, or 10.0 μM for at least 3 min between trials. The ionic strength was held constant at 180 mM in all solutions.

Mechanical Measurements—Pilot tests showed that OM was difficult to wash out of the multicellular preparations. Each preparation was therefore exposed to only one concentration of OM (0, 0.1, 1.0, or 10 μM). Specimens were initially activated in a solution with a *p*Ca value of 4.5. Once force reached steady state, the rate of tension recovery, k_{tr}, was measured by rapidly shortening the preparation by 20%, holding it at the short length for 20 ms, and then re-stretching the preparation to its original length. The k_{tr} was subsequently calculated by fitting the portion of the force record immediately after the re-stretch with a single exponential function of the form $F(t) = A + B(1 - \exp(-k_{tr}t))$. In this equation, $F(t)$ is the force at time t, and A and B are constants. Calcium sensitivity (pCa_{50}) was determined by repeating the force measurements with different solutions that had *p*Ca values in the range 9.0 to 5.0. pCa_{50} values were calculated by fitting the resulting data to a modified Hill equation of the form $F = F_{pas} + F_{Ca}([Ca^{2+}]^n/([Ca^{2+}]^n + [Ca^{2+}_{50}]^n))$, where F_{pas} is the force measured in *p*Ca 9.0 solution; F_{Ca} is Ca^{2+}-activated force; n is the Hill coefficient, and $[Ca^{2+}_{50}]^n$ is the free Ca^{2+} concentration required to develop half the maximum Ca^{2+}-dependent force.

Statistics for Muscle Mechanics on Human Samples—Experiments were performed using a total of 46 multicellular preparations from eight hearts. Data were analyzed using linear mixed models that allowed for the fact that multiple samples were analyzed from each heart. Compound symmetry was assumed for the covariance structure, and post-hoc analyses were performed using Tukey-Kramer corrections. p values less than 0.05 were considered significant. Data are reported as mean $\pm$ S.E.

Author Contributions—C. M. Y. designed the research; A. M. S., W. T., C. A. B., C. M. F., W. C. U., M. J. P., and C. M. Y. performed the research; A. M. S., W. T., C. A. B., C. M. F., W. C. U., M. J. P., K. S. C., and C. M. Y. analyzed the data; A. M. S., C. A. B., W. T., M. J. P., K. S. C., and C. M. Y. wrote paper. All authors approved the final version of the manuscript.

Acknowledgment—We thank Dr. Don Winkelmann, Rutgers University, for sharing his expertise on the adenovirus-based C_2C_{12} expression system.

References

1. Braunwald, E. (2013) Research advances in heart failure: a compendium. *Circ. Res.* **113,** 633–645
2. Roger, V. L., Go, A. S., Lloyd-Jones, D. M., Benjamin, E. J., Berry, J. D., Borden, W. B., Bravata, D. M., Dai, S., Ford, E. S., Fox, C. S., Fullerton, H. J., Gillespie, C., Hailpern, S. M., Heit, J. A., Howard, V. J., *et al.* (2012) Heart disease and stroke statistics–2012 update: a report from the American Heart Association. *Circulation* **125,** e2–e220
3. Teerlink, J. R., Metra, M., Zacà, V., Sabbah, H. N., Cotter, G., Gheorghiade, M., and Cas, L. D. (2009) Agents with inotropic properties for the management of acute heart failure syndromes. Traditional agents and beyond. *Heart Fail. Rev.* **14,** 243–253
4. Kass, D. A., and Solaro, R. J. (2006) Mechanisms and use of calcium-sensitizing agents in the failing heart. *Circulation* **113,** 305–315
5. Petersen, J. W., and Felker, G. M. (2008) Inotropes in the management of acute heart failure. *Crit. Care Med.* **36,** S106–S111
6. Malik, F. I., Hartman, J. J., Elias, K. A., Morgan, B. P., Rodriguez, H., Brejc, K., Anderson, R. L., Sueoka, S. H., Lee, K. H., Finer, J. T., Sakowicz, R., Baliga, R., Cox, D. R., Garard, M., Godinez, G., *et al.* (2011) Cardiac myosin activation: a potential therapeutic approach for systolic heart failure. *Science* **331,** 1439–1443
7. Batters, C., Veigel, C., Homsher, E., and Sellers, J. R. (2014) To understand muscle you must take it apart. *Front. Physiol.* **5,** 90
8. Moss, R. L., Fitzsimons, D. P., and Ralphe, J. C. (2015) Cardiac MyBP-C regulates the rate and force of contraction in mammalian myocardium. *Circ. Res.* **116,** 183–192
9. Sheikh, F., Lyon, R. C., and Chen, J. (2014) Getting the skinny on thick filament regulation in cardiac muscle biology and disease. *Trends Cardiovasc. Med.* **24,** 133–141
10. Málnási-Csizmadia, A., and Kovács, M. (2010) Emerging complex pathways of the actomyosin powerstroke. *Trends Biochem. Sci.* **35,** 684–690
11. Geeves, M. A. (2016) The ATPase mechanism of myosin and actomyosin. *Biopolymers* **105,** 483–491
12. Trivedi, D. V., Muretta, J. M., Swenson, A. M., Davis, J. P., Thomas, D. D., and Yengo, C. M. (2015) Direct measurements of the coordination of lever arm swing and the catalytic cycle in myosin V. *Proc. Natl. Acad. Sci. U.S.A.* **112,** 14593–14598
13. Muretta, J. M., Rohde, J. A., Johnsrud, D. O., Cornea, S., and Thomas, D. D. (2015) Direct real-time detection of the structural and biochemical events in the myosin power stroke. *Proc. Natl. Acad. Sci. U.S.A.* **112,** 14272–14277
14. Wulf, S. F., Ropars, V., Fujita-Becker, S., Oster, M., Hofhaus, G., Trabuco, L. G., Pylypenko, O., Sweeney, H. L., Houdusse, A. M., and Schröder, R. R. (2016) Force-producing ADP state of myosin bound to actin. *Proc. Natl. Acad. Sci. U.S.A.* **113,** E1844–E1852
15. Siemankowski, R. F., Wiseman, M. O., and White, H. D. (1985) ADP dissociation from actomyosin subfragment 1 is sufficiently slow to limit the unloaded shortening velocity in vertebrate muscle. *Proc. Natl. Acad. Sci. U.S.A.* **82,** 658–662
16. Brizendine, R. K., Alcala, D. B., Carter, M. S., Haldeman, B. D., Facemyer, K. C., Baker, J. E., and Cremo, C. R. (2015) Velocities of unloaded muscle filaments are not limited by drag forces imposed by myosin cross-bridges. *Proc. Natl. Acad. Sci. U.S.A.* **112,** 11235–11240
17. Haldeman, B. D., Brizendine, R. K., Facemyer, K. C., Baker, J. E., and Cremo, C. R. (2014) The kinetics underlying the velocity of smooth muscle myosin filament sliding on actin filaments *in vitro*. *J. Biol. Chem.* **289,** 21055–21070
18. Cleland, J. G., Teerlink, J. R., Senior, R., Nifontov, E. M., Mc Murray, J. J., Lang, C. C., Tsyrlin, V. A., Greenberg, B. H., Mayet, J., Francis, D. P., Shaburishvili, T., Monaghan, M., Saltzberg, M., Neyses, L., Wasserman, S. M., *et al.* (2011) The effects of the cardiac myosin activator, omecamtiv mecarbil, on cardiac function in systolic heart failure: a double-blind,

placebo-controlled, crossover, dose-ranging phase 2 trial. *Lancet* **378,** 676–683
19. Greenberg, B. H., Chou, W., Saikali, K. G., Escandón, R., Lee, J. H., Chen, M. M., Treshkur, T., Megreladze, I., Wasserman, S. M., Eisenberg, P., Malik, F. I., Wolff, A. A., and Shaburishvili, T. (2015) Safety and tolerability of omecamtiv mecarbil during exercise in patients with ischemic cardiomyopathy and angina. *JACC Heart Fail.* **3,** 22–29
20. Teerlink, J. R., Felker, G. M., McMurray, J. J., Ponikowski, P., Metra, M., Filippatos, G. S., Ezekowitz, J. A., Dickstein, K., Cleland, J. G., Kim, J. B., Lei, L., Knusel, B., Wolff, A. A., Malik, F. I., Wasserman, S. M., and ATOMIC-AHF Investigators. (2016) Acute treatment with omecamtiv mecarbil to increase contractility in acute heart failure: the ATOMIC-AHF study. *J. Am. Coll. Cardiol.* **67,** 1444–1455
21. Utter, M. S., Ryba, D. M., Li, B. H., Wolska, B. M., and Solaro, R. J. (2015) Omecamtiv mecarbil, a cardiac myosin activator, increases Ca^{2+} sensitivity in myofilaments with a dilated cardiomyopathy mutant tropomyosin E54K. *J. Cardiovasc. Pharmacol.* **66,** 347–353
22. Nagy, L., Kovacs, A., Bodi, B., Pasztor, E. T., Fulop, G. A., Toth, A., Edes, I., and Papp, Z. (2015) The novel cardiac myosin activator omecamtiv mecarbil increases the calcium sensitivity of force production in isolated cardiomyocytes and skeletal muscle fibres of the rat. *Br. J. Pharmacol.* **2015,** e13235
23. Mamidi, R., Gresham, K. S., Li, A., dos Remedios, C. G., and Stelzer, J. E. (2015) Molecular effects of the myosin activator omecamtiv mecarbil on contractile properties of skinned myocardium lacking cardiac myosin binding protein-C. *J. Mol. Cell. Cardiol.* **85,** 262–272
24. Liu, Y., White, H. D., Belknap, B., Winkelmann, D. A., and Forgacs, E. (2015) Omecamtiv mecarbil modulates the kinetic and motile properties of porcine β-cardiac myosin. *Biochemistry* **54,** 1963–1975
25. Winkelmann, D. A., Forgacs, E., Miller, M. T., and Stock, A. M. (2015) Structural basis for drug-induced allosteric changes to human β-cardiac myosin motor activity. *Nat. Commun.* **6,** 7974
26. Aksel, T., Choe Yu, E., Sutton, S., Ruppel, K. M., and Spudich, J. A. (2015) Ensemble force changes that result from human cardiac myosin mutations and a small-molecule effector. *Cell Rep.* **11,** 910–920
27. Wang, Y., Ajtai, K., and Burghardt, T. P. (2014) Analytical comparison of natural and pharmaceutical ventricular myosin activators. *Biochemistry* **53,** 5298–5306
28. Smith, D. A., and Geeves, M. A. (1995) Strain-dependent cross-bridge cycle for muscle. *Biophys. J.* **69,** 524–537
29. Albet-Torres, N., Bloemink, M. J., Barman, T., Candau, R., Frölander, K., Geeves, M. A., Golker, K., Herrmann, C., Lionne, C., Piperio, C., Schmitz, S., Veigel, C., and Månsson, A. (2009) Drug effect unveils inter-head cooperativity and strain-dependent ADP release in fast skeletal actomyosin. *J. Biol. Chem.* **284,** 22926–22937
30. Van Dijk, J., Fernandez, C., and Chaussepied, P. (1998) Effect of ATP analogues on the actin-myosin interface. *Biochemistry* **37,** 8385–8394
31. Chalovich, J. M., Stein, L. A., Greene, L. E., and Eisenberg, E. (1984) Interaction of isozymes of myosin subfragment 1 with actin: effect of ionic strength and nucleotide. *Biochemistry* **23,** 4885–4889
32. Greene, L. E., and Eisenberg, E. (1978) Formation of a ternary complex: actin, 5′-adenylyl imidodiphosphate, and the subfragments of myosin. *Proc. Natl. Acad. Sci. U.S.A.* **75,** 54–58
33. Uyeda, T. Q., Kron, S. J., and Spudich, J. A. (1990) Myosin step size. Estimation from slow sliding movement of actin over low densities of heavy meromyosin. *J. Mol. Biol.* **214,** 699–710
34. Moore, J. R., Krementsova, E. B., Trybus, K. M., and Warshaw, D. M. (2001) Myosin V exhibits a high duty cycle and large unitary displacement. *J. Cell Biol.* **155,** 625–635
35. De La Cruz, E. M., Wells, A. L., Sweeney, H. L., and Ostap, E. M. (2000) Actin and light chain isoform dependence of myosin V kinetics. *Biochemistry* **39,** 14196–14202
36. Nag, S., Sommese, R. F., Ujfalusi, Z., Combs, A., Langer, S., Sutton, S., Leinwand, L. A., Geeves, M. A., Ruppel, K. M., and Spudich, J. A. (2015) Contractility parameters of human β-cardiac myosin with the hypertrophic cardiomyopathy mutation R403Q show loss of motor function. *Sci. Adv.* **1,** e1500511
37. Sommese, R. F., Sung, J., Nag, S., Sutton, S., Deacon, J. C., Choe, E., Leinwand, L. A., Ruppel, K., and Spudich, J. A. (2013) Molecular consequences of the R453C hypertrophic cardiomyopathy mutation on human β-cardiac myosin motor function. *Proc. Natl. Acad. Sci. U.S.A.* **110,** 12607–12612
38. Sakamoto, T., Yildez, A., Selvin, P. R., and Sellers, J. R. (2005) Step-size is determined by neck length in myosin V. *Biochemistry* **44,** 16203–16210
39. Moore, J. R., Krementsova, E. B., Trybus, K. M., and Warshaw, D. M. (2004) Does the myosin V neck region act as a lever? *J. Muscle Res. Cell Motil.* **25,** 29–35
40. Ruff, C., Furch, M., Brenner, B., Manstein, D. J., and Meyhöfer, E. (2001) Single-molecule tracking of myosins with genetically engineered amplifier domains. *Nat. Struct. Biol.* **8,** 226–229
41. Noguchi, T., Camp, P., Jr, Alix, S. L., Gorga, J. A., Begin, K. J., Leavitt, B. J., Ittleman, F. P., Alpert, N. R., LeWinter, M. M., and VanBuren, P. (2003) Myosin from failing and non-failing human ventricles exhibit similar contractile properties. *J. Mol. Cell. Cardiol.* **35,** 91–97
42. Fewell, J. G., Hewett, T. E., Sanbe, A., Klevitsky, R., Hayes, E., Warshaw, D., Maughan, D., and Robbins, J. (1998) Functional significance of cardiac myosin essential light chain isoform switching in transgenic mice. *J. Clin. Invest.* **101,** 2630–2639
43. Bakkehaug, J. P., Kildal, A. B., Engstad, E. T., Boardman, N., Næsheim, T., Rønning, L., Aasum, E., Larsen, T. S., Myrmel, T., and How, O. J. (2015) Myosin activator omecamtiv mecarbil increases myocardial oxygen consumption and impairs cardiac efficiency mediated by resting myosin ATPase activity. *Circ. Heart Fail.* **8,** 766–775
44. De La Cruz, E. M., and Ostap, E. M. (2009) Kinetic and equilibrium analysis of the myosin ATPase. *Methods Enzymol.* **455,** 157–192
45. Wang, Q., Moncman, C. L., and Winkelmann, D. A. (2003) Mutations in the motor domain modulate myosin activity and myofibril organization. *J. Cell Sci.* **116,** 4227–4238
46. Lin, T., Tang, N., and Ostap, E. M. (2005) Biochemical and motile properties of Myo1b splice isoforms. *J. Biol. Chem.* **280,** 41562–41567
47. Pardee, J. D., and Spudich, J. A. (1982) Purification of muscle actin. *Methods Enzymol.* **85,** 164–181
48. Previs, M. J., Beck Previs, S., Gulick, J., Robbins, J., and Warshaw, D. M. (2012) Molecular mechanics of cardiac myosin-binding protein C in native thick filaments. *Science* **337,** 1215–1218
49. Dosé, A. C., Ananthanarayanan, S., Moore, J. E., Burnside, B., and Yengo, C. M. (2007) Kinetic mechanism of human myosin IIIA. *J. Biol. Chem.* **282,** 216–231
50. Dosé, A. C., Ananthanarayanan, S., Moore, J. E., Corsa, A. C., Burnside, B., and Yengo, C. M. (2008) The kinase domain alters the kinetic properties of the myosin IIIA motor. *Biochemistry* **47,** 2485–2496
51. Quintero, O. A., Moore, J. E., Unrath, W. C., Manor, U., Salles, F. T., Grati, M., Kachar, B., and Yengo, C. M. (2010) Intermolecular autophosphorylation regulates myosin IIIa activity and localization in parallel actin bundles. *J. Biol. Chem.* **285,** 35770–35782
52. De La Cruz, E. M., Sweeney, H. L., and Ostap, E. M. (2000) ADP inhibition of myosin V ATPase activity. *Biophys. J.* **79,** 1524–1529
53. Kron, S. J., Toyoshima, Y. Y., Uyeda, T. Q., and Spudich, J. A. (1991) Assays for actin sliding movement over myosin-coated surfaces. *Methods Enzymol.* **196,** 399–416
54. Meijering, E., Dzyubachyk, O., and Smal, I. (2012) Methods for cell and particle tracking. *Methods Enzymol.* **504,** 183–200
55. Trybus, K. M. (2000) Biochemical studies of myosin. *Methods* **22,** 327–335
56. Blair, C. A., Haynes, P., Campbell, S. G., Chung, C., Mitov, M. I., Dennis, D., Bonnell, M. R., Hoopes, C. W., Guglin, M., Campbell, K. S. (2016) A protocol for collecting human cardiac tissue for research. *VAD J.* **2,** 11/12
57. Haynes, P., Nava, K. E., Lawson, B. A., Chung, C. S., Mitov, M. I., Campbell, S. G., Stromberg, A. J., Sadayappan, S., Bonnell, M. R., Hoopes, C. W., and Campbell, K. S. (2014) Transmural heterogeneity of cellular level power output is reduced in human heart failure. *J. Mol. Cell. Cardiol.* **72,** 1–8
58. Campbell, K. S., and Moss, R. L. (2003) SLControl: PC-based data acquisition and analysis for muscle mechanics. *Am. J. Physiol. Heart Circ. Physiol.* **285,** H2857–H2864

Omecamtiv Mecarbil Enhances the Duty Ratio of Human β-Cardiac Myosin Resulting in Increased Calcium Sensitivity and Slowed Force Development in Cardiac Muscle

Anja M. Swenson, Wanjian Tang, Cheavar A. Blair, Christopher M. Fetrow, William C. Unrath, Michael J. Previs, Kenneth S. Campbell and Christopher M. Yengo

J. Biol. Chem. 2017, 292:3768-3778.
doi: 10.1074/jbc.M116.748780 originally published online January 12, 2017

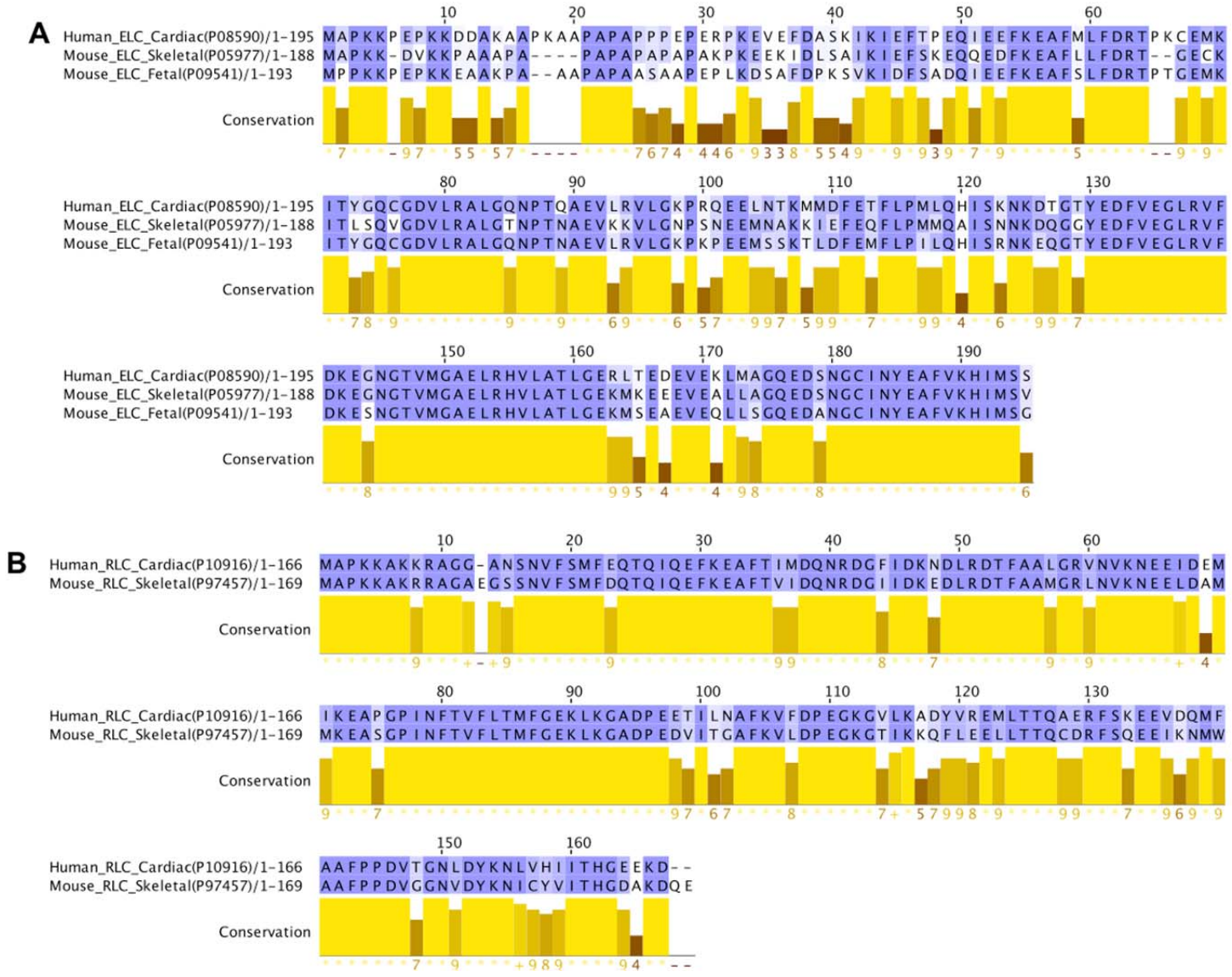

Figure S1: Sequence alignments of murine essential and regulatory light chains with the ventricular human cardiac isoforms. A) The two murine essential light chains present in our M2β-S1 construct, myosin light chain 1/3 (UniProt - P05977) and myosin light chain 4 (Uni-Prot-P09541), were 75% and 79% identical and 83% and 91% similar, respectively, to the human myosin light chain 3 (P08590). B) The murine regulatory light chain present in our M2-βS1 construct, myosin regulatory light chain 2 (UniProt - P97457), is 74% identical and 87% similar to the human cardiac muscle regulatory light chain 2 (P10916). The sequences were aligned using Jalview with the similarity of each residue colored based on BLOSUM62 score.